The elliptical model of two-dimensional vortex dynamics. II: Disturbance equations

David G. Dritschel
Department of Applied Mathematics and Theoretical Physics, University of Cambridge, Silver Street, Cambridge CB3 9EW, England

Bernard Legras
Laboratoire de Météorologie Dynamique du CNRS, École Normale Supérieure, 24 rue Lhomond, 75231 Paris Cedex 05, France

(Received 6 February 1990; accepted 6 December 1990)

In Part I [Phys. Fluids A 3, 845 (1991)] approximate equations were developed that describe the basic evolution of vortices in a general strain field. These equations take the form of a set of coupled, nonlinear ordinary differential equations describing the time evolution of the centroids, aspect ratios, and orientations of a nested set of elliptical contours representing each vortex. Here, in Part II, the model is extended to include disturbances to the elliptical shape of each contour, disturbances that are excited naturally by the interaction with other vortices. This interaction is worked out explicitly for the first time. The final equations obtained decouple into sets of equations for each mode symmetry, allowing for a very simple description of the disturbance evolution. Numerical tests show remarkable agreement between the elliptical model and the full equations of motion in four problems: (1) the equilibrium contour shapes of a multicontour family of vortices, (2) the linear stability of this family, (3) the equilibrium, nonelliptical shapes of two corotating vortex patches, and (4) the interaction between two symmetrical vortex patches, including merging.

I. MODEL ASSUMPTIONS

We begin with the approximate model developed in Part I.[1] In this model, each vortex is represented by a stack or pile of elliptical patches of uniform vorticity, with no mathematical limitation being placed on their number. Evolution equations are derived for the centroid, aspect ratio, and orientation of each ellipse by retaining just the part of the local velocity field that preserves the elliptical form. The velocity field itself consists of an arbitrary external straining flow and contributions from every ellipse within every vortex.

The imposition of a basic elliptical shape to each contour is not equivalent to a formal perturbation series development. *A posteriori*, one must rely on extensive comparisons against contour dynamics to estimate the magnitude of the error. There are two principal sources of error. One arises from mismatched foci of the ellipses comprising a given vortex. The instantaneous motion of a confocal set of ellipses may be calculated exactly, in the absence of other vortices, although the time evolution will normally lead to mismatched foci. A second source of error arises from the interactions between separated vortices. This interaction leads predominantly to elliptical deformations, but there are also higher order deformations which are ignored in the basic model.

In Part II, we incorporate higher-order deformations. We assume, however, that their amplitudes are small, so that we can ignore quadratic disturbance interactions. Thus, there is no feedback on the basic elliptical evolution of the contours. Within a given vortex, disturbances having different azimuthal symmetries are assumed to be decoupled from each other, an approximation that requires approximate confocality of the basic ellipses (there is no coupling for a confocal set of ellipses). Between separate vortices, the primary source of disturbance excitation is assumed to arise from the basic elliptical interaction of one vortex with the disturbances of the other. The neglected disturbance–disturbance interaction can be estimated and is substantially weaker as long as the vortices remain well separated.

II. PROPERTIES OF A SINGLE, DISTURBED ELLIPSE

It is sufficient to consider irrotational or boundary-deforming disturbances, since other types of disturbances can be rendered irrotational by a suitable choice of the basic flow. The streamfunction, $\psi(x,y,t)$, due to a disturbed elliptical contour of semimajor axis a, semiminor axis b, and containing vorticity ω in excess of that in the surrounding flow, is split into a basic part $\bar{\psi}(x,y,t)$ and a disturbance part $\hat{\psi}(x,y,t)$. Both $\bar{\psi}(x,y,t)$ and $\hat{\psi}(x,y,t)$ have different expressions in the interior and the exterior, owing to the discontinuous vorticity at the boundary of the ellipse. The basic-state streamfunction in the interior of an ellipse, oriented with semimajor and semiminor axes coincident with the positive x and y axes, is

$$\bar{\psi} = \frac{\omega}{2(1+\lambda)}(\lambda x^2 + y^2), \tag{1}$$

where $\lambda \equiv b/a$ is the aspect ratio of the ellipse (see, e.g., Ref. 2, Art. 159). In the exterior, the streamfunction is most simply expressed in terms of elliptical coordinates (ξ,η), which are related to the original Cartesian ones by

 0899-8213/91/050855-15$02.00

$x = c\cosh\xi\cos\eta$ and $y = c\sinh\xi\sin\eta$

($c \equiv \sqrt{a^2 - b^2}$). Then,

$$\bar{\psi} = \kappa(\xi + \tfrac{1}{2}e^{-2\xi}\cos 2\eta) + K, \tag{2}$$

where $\kappa \equiv \frac{1}{2}\omega ab$ and K depends on ω, a, and b, but not on ξ or η. This constant is unimportant and may be ignored forthwith.

For the disturbance, considered to be an irrotational response to the deformation of the boundary away from the boundary, the interior disturbance streamfunction may take the general form

$$\hat{\psi} = C\cosh m\xi\cos m\eta + D\sinh m\xi\sin m\eta, \tag{3}$$

with $C(t)$ and $D(t)$ as yet undetermined. We require that the velocity, whose components are proportional to $\partial\psi/\partial\eta$ and $\partial\psi/\partial\xi$, be continuous across the boundary. Continuity of $\partial\psi/\partial\eta$, to leading order in disturbance amplitude, requires that the exterior disturbance streamfunction be of the form

$$\hat{\psi} = e^{-m\xi}(E\cos m\eta + F\sin m\eta) \tag{4}$$

with

$$E = Ce^{m\bar{\Gamma}}\cosh m\bar{\Gamma}, \quad F = De^{m\bar{\Gamma}}\sinh m\bar{\Gamma}, \tag{5}$$

where $\xi = \bar{\Gamma}$ gives the undisturbed elliptical boundary. In terms of the eccentricity ϵ note that

$$e^{-\bar{\Gamma}} = \epsilon \equiv \sqrt{(1-\lambda)/(1+\lambda)}.$$

The actual disturbed boundary is denoted by

$$\Gamma(\eta,t) = \bar{\Gamma}(t) + \hat{\Gamma}(\eta,t), \quad \hat{\Gamma} \ll \bar{\Gamma}.$$

Continuity of $\partial\psi/\partial\xi$, which to first order in disturbance amplitude is

$$\frac{\partial\bar{\psi}}{\partial\xi}(\bar{\Gamma},\eta) + \hat{\Gamma}\frac{\partial^2\bar{\psi}}{\partial^2\xi}(\bar{\Gamma},\eta) + \frac{\partial\hat{\psi}}{\partial\xi}(\bar{\Gamma},\eta),$$

implies [using (1)–(5)] that

$$\omega\hat{\Gamma}\bar{h}^2 = -me^{m\bar{\Gamma}}(C\cos m\eta + D\sin m\eta),$$

where $\bar{h}^2 \equiv a^2\sin^2\eta + b^2\cos^2\eta$. Therefore, setting

$$\rho(\eta,t) \equiv \hat{\Gamma}\bar{h}^2 = A\cos m\eta + B\sin m\eta, \tag{6}$$

we obtain

$$C = -(\omega/m)Ae^{-m\bar{\Gamma}},$$

$$D = -(\omega/m)Be^{-m\bar{\Gamma}}, \tag{7a}$$

$$E = -(\omega/m)A\cosh m\bar{\Gamma}, \tag{7b}$$

$$F = -(\omega/m)B\sinh m\bar{\Gamma}.$$

Note, $\bar{h}\hat{\Gamma}$ is a small normal distance displacement outwards from the undisturbed elliptical boundary.

III. THE LINEAR DISTURBANCE EVOLUTION EQUATIONS

We next derive the general evolution equations satisfied by $A(t)$ and $B(t)$ in (6). Here, we implicitly take into account the presence of other contours (and vortices) as well as an imposed external straining flow, but leave explicit algebraic computations to Secs. IV and V.

The starting point is the equation governing the motion of a particle in the time-varying elliptical coordinates of a given contour derived in Part I, Sec. II. Let $Z = X + iY$ be the centroid of the ellipse, $c = \sqrt{a^2 - b^2}$ is the half-distance between the foci, and ϕ is the orientation of the ellipse relative to fixed axes. With respect to these fixed axes, the position of a particle is given by

$$z = x + iy = Z + ce^{i\phi}\cosh w,$$

where $w = \xi + i\eta$ is the complex elliptical coordinate of the particle. The motion of this particle is described by the equation

$$c^2|\sinh w|^2\dot{w} = i\left(\frac{\partial\psi}{\partial w}\right)^* - \dot{Z}e^{-i\phi}c\sinh w^* - (c\dot{c} + i\dot{\phi}c^2)\cosh w\sinh w^*, \tag{8}$$

where a dot stands for d/dt, $\psi = \psi(w,t)$, and * denotes complex conjugation.

The basic flow evolution for the Z's, λ's, and ϕ's is obtained from the real part of (8) evaluated along the undisturbed contour, as described in Part I [see in particular Eqs. (5) and (8) in Part I]. An important quantity for the disturbance evolution, however, is contained within the imaginary part of (8) evaluated along the undisturbed contour. This imaginary part yields the equation

$$\bar{h}^2\bar{\Omega} = \frac{\partial\bar{\psi}}{\partial\xi}(\bar{\Gamma},\eta) + \frac{1}{2}c\dot{c}\sin 2\eta - R^2\dot{\phi} + \Re[\dot{Z}e^{-i\phi}]a\sin\eta - \Im[\dot{Z}e^{-i\phi}]b\cos\eta, \tag{9}$$

where $R^2 \equiv ab$ and $\bar{\Omega} \equiv \overline{d\eta/dt}$. Here, $\bar{\Omega}$ is a basic state quantity determined much in the same way as $\dot{Z}$, $\dot{\lambda}$, and $\dot{\phi}$ were in Part I (details may be found in Appendix A).

The disturbance equations are contained within the real part of (8) evaluated along the *disturbed* contour,

$$c^2|\sinh(\Gamma + i\eta)|^2\dot{\Gamma} = -\frac{\partial\psi}{\partial\eta}(\Gamma,\eta) - \frac{1}{2}c\dot{c}\sinh 2\Gamma - \frac{1}{2}c^2\dot{\phi}\sin 2\eta - \Re[\dot{Z}e^{-i\phi}]c\sinh\Gamma\cos\eta - \Im[\dot{Z}e^{-i\phi}]c\cosh\Gamma\sin\eta, \tag{10}$$

and are isolated by linearizing this equation about the basic flow. The algebraic manipulations are lengthy, and only a brief sketch is given here. One uses the relation $d\bar{\Gamma}/dt = -(\dot{c}/c)\tanh 2\bar{\Gamma}$, which expresses conservation of area, expands $d\hat{\Gamma}/dt$ into $\partial\hat{\Gamma}/\partial t + \bar{\Omega}\,\partial\hat{\Gamma}/\partial\eta$, and substitutes $\hat{\Gamma} = \rho/\bar{h}^2$ from (6) to find the remarkably simple result

$$\frac{\partial\rho}{\partial t} + \frac{\partial(\bar{\Omega}\rho)}{\partial\eta} = -\frac{\partial\psi_{>2}}{\partial\eta}(\bar{\Gamma},\eta). \tag{11}$$

Here, $\psi_{>2} \equiv \psi - \psi_{\leq 2}$, which is the streamfunction exclusive of elliptical deformations. Using the expression (6) for ρ and the fact that $\bar{\Omega}$ is independent of η (see Appendix A), (11) becomes

$$(\dot{A} + m\bar{\Omega}B)\cos m\eta + (\dot{B} - m\bar{\Omega}A)\sin m\eta = -\frac{\partial\psi_m}{\partial\eta}(\bar{\Gamma},\eta), \tag{12}$$

for each integer $m > 2$. Here ψ_m is the streamfunction restricted to the $\cos m\eta$ and $\sin m\eta$ components.

IV. NESTED ELLIPSES

In this section, we explicitly calculate the contributions to $\dot{A}$ and $\dot{B}$ from the same and other contours within a single vortex. For a single ellipse, the analysis of Sec. II shows that a small boundary disturbance of the form (6) has associated with it a streamfunction response $\hat{\psi}(\overline{\Gamma},\eta)$ of the same azimuthal symmetry, say m. Within this linear analysis, superposed disturbances having different azimuthal symmetries $n \neq m$ do not interact with each other.[3] Nor in fact do they interact in the case of a confocal set of embedded ellipses (see below). Hence, coupling between modes of different symmetry only occurs as a result of mismatched foci.

In the following analysis, we ignore this coupling but retain the leading-order effects of mismatched foci by computing the nonelliptical deformations excited by the basic set of ellipses. If we were to take into account the coupling of disturbances having different symmetries, for consistency we would then be forced to consider also the modification of the basic flow by disturbances, and this does not seem justifiable in light of the numerical results presented in Sec. VIII.

There are four sources of disturbance excitation: (i) self-excitation, (ii) interaction with disturbances on exterior ellipses, (iii) interaction with disturbances on interior ellipses, and (iv) generation by mismatched foci. The first three sources arise from existing disturbances while the latter arises from the basis set of ellipses. This latter source is the first of two that we will encounter that pick up the nonelliptical part of the velocity field discarded in obtaining the basic model.

We turn first to the contribution from exterior ellipses, (ii), the simplest to compute. The auto-contribution (i) can be obtained as a special case of (ii) or indeed of (iii). The disturbance streamfunction interior to the advecting ellipse $(Z',\lambda',\phi',A',B')$ due to a single azimuthal wave number m is given by (3) (supplemented by primes):

$$\hat{\psi} = C' \cosh m\xi' \cos m\eta' + D' \sinh m\xi' \sin m\eta'$$
$$= \Re[(C' - iD')\cosh mw'].$$

The coordinate system of the advectee is linked to that of the advector by the relation

$$z = Z + ce^{i\phi} \cosh w = Z' + c'e^{i\phi'} \cosh w',$$

giving

$$\cosh w' = \Lambda \cosh w + (Z - Z')/2\nu',$$

where we have introduced the notation $2\nu' \equiv c'e^{i\phi'}$ and $\Lambda \equiv \nu/\nu'$. The cos $m\eta$ and sin $m\eta$ components of $\hat{\psi}$ are readily seen to be

$$\Re[(C' - iD')\Lambda^m \cosh mw],$$

which is

$$(c/c')^m\{(C' \cos m(\phi - \phi') + D' \sin m(\phi - \phi'))$$
$$\times \cosh m\xi \cos m\eta$$
$$+ (D' \cos m(\phi - \phi') + C' \sin m(\phi - \phi'))$$
$$\times \sinh m\xi \sin m\eta\}.$$

Of course, there also exist cos $n\eta$ and sin $n\eta$ components of $\hat{\psi}$ for $n < m$, but these vanish for a confocal set of contours, for then $\Lambda = 1$ and $Z = Z'$ (in this case $\cosh mw = \cosh mw'$). These terms are therefore neglected here. (Otherwise, disturbances would bring about a change to the basic flow through the $n = 1$ and 2 components of $\hat{\psi}$.) Using (7a), one then finds that the contribution to $\dot{A}$ and $\dot{B}$ is

$$\dot{A} \leftarrow + \omega'(c/c')^m e^{-m\overline{\Gamma}'}(B' \cos m(\phi - \phi')$$
$$- A' \sin m(\phi - \phi'))\sinh m\overline{\Gamma}', \quad (13a)$$
$$\dot{B} \leftarrow - \omega'(c/c')^m e^{-m\overline{\Gamma}'}(A' \cos m(\phi - \phi')$$
$$+ B' \sin m(\phi - \phi'))\cosh m\overline{\Gamma}'. \quad (13b)$$

Next consider case (iii) when the advecting ellipse $(Z',\lambda',\phi',A',B')$ is interior to the advectee. In this case, the disturbance streamfunction is given by (4) (with primes):

$$\hat{\psi} = e^{-m\xi'}(E' \cos m\eta' + F' \sin m\eta')$$
$$= \Re[(E' + iF')e^{-mw'}];$$

thus

$$-\frac{\partial\hat{\psi}}{\partial\eta} = \Im\left[(E' + iF')\frac{de^{-mw'}}{dw}\right]. \quad (14)$$

To extract the cos $m\eta$ and sin $m\eta$ components, it is necessary to calculate the following contour integrals taken around the undisturbed boundary of the advectee $\xi = \overline{\Gamma}$:

$$I_s = -\frac{1}{\pi}\int_{\overline{\Gamma}}^{\overline{\Gamma}+2i\pi} \frac{de^{-mw'}}{dw} \cosh m(w - \overline{\Gamma})dw$$
$$= +\frac{m}{\pi}\int_{\overline{\Gamma}}^{\overline{\Gamma}+2i\pi} e^{-mw'} \sinh m(w - \overline{\Gamma})dw, \quad (15a)$$
$$I_c = -\frac{1}{\pi}\int_{\overline{\Gamma}}^{\overline{\Gamma}+2i\pi} \frac{de^{-mw'}}{dw} \sinh m(w - \overline{\Gamma})dw$$
$$= +\frac{m}{\pi}\int_{\overline{\Gamma}}^{\overline{\Gamma}+2i\pi} e^{-mw'} \cosh m(w - \overline{\Gamma})dw. \quad (15b)$$

Using the integral expressions developed in Part I, Sec. V along with a few additional straightforward computations, it is possible to show that

$$I_s = I_c = im\Lambda^{-m}e^{-m\overline{\Gamma}}, \quad (16)$$

which implies that the cos $m\eta$ and sin $m\eta$ components of $de^{-mw'}/dw$ can be encapsulated in the particularly simple expression

$$-m\Lambda^{-m}e^{-mw}.$$

Again, there are also cos $n\eta$ and sin $n\eta$ components for $n \neq m$, but these vanish for a confocal set of ellipses and so are neglected in this analysis. (Again, otherwise we would have to take into account the change to the basic flow by the $n = 1$ and 2 components of $\hat{\psi}$.) Using (7b) we can then conclude that the contribution to $\dot{A}$ and $\dot{B}$ is

$$\dot{A} \leftarrow + \omega'(c'/c)^m e^{-m\overline{\Gamma}}(B' \cos m(\phi - \phi')$$
$$- A' \sin m(\phi - \phi'))\sinh m\overline{\Gamma}', \quad (17a)$$
$$\dot{B} \leftarrow - \omega'(c'/c)^m e^{-m\overline{\Gamma}}(A' \cos m(\phi - \phi')$$
$$+ B' \sin m(\phi - \phi'))\cosh m\overline{\Gamma}'. \quad (17b)$$

Finally, we consider the contribution from mismatched foci within the basic set of ellipses. In Part I, it is proved that an exterior ellipse, like an external straining flow, induces

only elliptical deformations on an interior ellipse, so there is no disturbance contribution in this case. However, an interior ellipse does generally induce nonelliptical deformations on an exterior ellipse—this is indeed the reason why the basic model is approximate. This source of disturbance excitation is calculated next.

From (12), it is clear that we have to consider the following two integrals:

$$I_m \equiv -\frac{1}{\pi}\int_0^{2\pi} \frac{\partial \bar{\psi}}{\partial \eta} \sin m\eta \, d\eta$$

$$= -\Im\left[\frac{1}{\pi}\int_{\bar{\Gamma}}^{\bar{\Gamma}+2i\pi} \frac{\partial \bar{\Psi}}{\partial w} \sinh m(w-\bar{\Gamma}) dw\right], \tag{18}$$

which is the contribution to $\dot{B}$, and

$$J_m \equiv -\frac{1}{\pi}\int_0^{2\pi} \frac{\partial \bar{\psi}}{\partial \eta} \cos m\eta \, d\eta$$

$$= -\Re\left[\frac{1}{\pi}\int_{\bar{\Gamma}}^{\bar{\Gamma}+2i\pi} \frac{\partial \bar{\Psi}}{\partial w} \cosh m(w-\bar{\Gamma}) dw\right], \tag{19}$$

which is the contribution to $\dot{A}$. Here, irrotationality permits us to use, advantageously, the complex extension of the streamfunction $\bar{\Psi}$, defined in Appendix A, Eq. (A6). In Part I, Sec. V, I_m and J_m are evaluated for $m = 1$ and 2 in order to obtain $\dot{Z}$, $\dot{\lambda}$, and $\dot{\phi}$ [for example, $\dot{\phi} = 2I_2/c^2$ — see Part I, Eq. (29)].

The details of the calculation may be found in Appendix B, since the calculation for $m > 2$ is not significantly different from that for $m \leqslant 2$ (described in Part I). For arbitrary m, however, it has not been possible to obtain a closed form expression for I_m and J_m (unless an approximation is made—see Appendix B). A symbolic calculation was necessary to produce the results, and these are listed for m up to 10 in Appendix B. In general, we have been able to determine that I_m and J_m are given by

$$J_m + iI_m = -i\kappa' \epsilon^m G_m(P,Q), \tag{20}$$

with $P \equiv 1/\Lambda = \nu'/\nu$ and $Q \equiv (Z' - Z)/\nu$, and where G_m is a polynomial in P and Q with integer coefficients. In terms of G_m, the contribution to $\dot{A}$ and $\dot{B}$, therefore, is

$$\dot{A} \leftarrow +\kappa' \epsilon^m \Im[G_m], \tag{21a}$$

$$\dot{B} \leftarrow -\kappa' \epsilon^m \Re[G_m]. \tag{21b}$$

V. SEPARATED ELLIPSES

The validity of the basic model depends also on well-separated vortices. For well-separated vortices, the interaction of disturbances on one vortex with those on another turns out to be small compared to the generation of disturbances by the nonelliptical part of the velocity field discarded in obtaining the basic model. (This is the second source of disturbance excitation arising from the basic set of ellipses.) As in the previous section, if we were to include disturbance interactions between separated ellipses, we would also be forced to include basic flow modifications caused by the disturbances. This does not appear justifiable at the present time—further remarks follow at the end of this section.

We begin by examining the effect of the basic elliptical shape of one contour, the "advector," on the disturbance evolution of another, the "advectee" (see Fig. 1 for definitions). The relevant integrals are I_m and J_m defined above in (18) and (19), with the understanding that the advector is not embedded within but separated from the advectee. To avoid the explicit appearance of elliptical functions of the third kind, an approximation is made that replaces the advector by a finite set of point vortices distributed along the line segment connecting the advector's foci [see Part I, Sec. VI, Eqs. (34) and (35)]. The true exterior velocity field of the advector that is needed for the calculation of I_m and J_m is very closely approximated in this way. Let $\kappa_\odot$ denote the strength of one of these point vortices and $z_\odot$ its position. Employing the method developed in Part I (Appendix B) to calculate integrals of this form, elementary algebra leads to the simple result

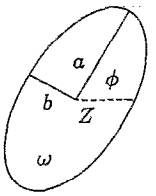

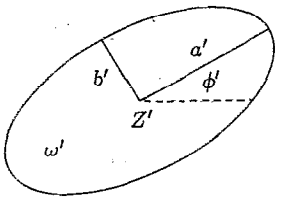

FIG. 1. A sketch of two interacting ellipses.

$$I_m = -2\kappa_\odot \cosh m\bar{\Gamma}\, \Re[e^{-m\breve{w}_\odot}], \tag{22a}$$

$$J_m = -2\kappa_\odot \sinh m\bar{\Gamma}\, \Im[e^{-m\breve{w}_\odot}], \tag{22b}$$

for each point vortex. Here, $\breve{w}_\odot$ is determined from the solution of

$$Z + ce^{i\phi} \cosh \breve{w}_\odot = z_\odot, \tag{23}$$

which is a quadratic equation for $e^{-\breve{w}_\odot}$.

For large separation distances,

$$|I_m \pm J_m| \approx 2\kappa_\odot \left(\frac{a \pm b}{2|Z - z_\odot|}\right)^m, \tag{24}$$

showing that disturbance excitation decreases rapidly with increasing azimuthal wave number.

One can equally well determine the contribution to $\dot{A}$ and $\dot{B}$ due to a disturbance riding on the advector, using $\partial\hat{\psi}/\partial\eta$ in place of $\partial\bar{\psi}/\partial\eta$ in (18) and (19). The procedure is again to approximate the advector by a finite set of point vortices, only now the point vortices are slightly disturbed from their basic positions between the advector's foci (in this way, the exterior velocity field of the disturbed contour can be accurately approximated). The full effect of the advector on the advectee then has the form already given in (22), only the $z_\odot$'s of each point vortex appearing in (23) depart slightly—by an amount proportional to the disturbance amplitude

on the advector—from their basic, undisturbed values. Thus, the effect of the advector's disturbances is only to slightly change the interaction between the contours, as can be seen most clearly from (24). (There would also be a basic flow modification, and this we wish to ignore. Consistency then requires that we ignore all effects of the advector's disturbances on the advectee.)

VI. THE COMPLETE ELLIPTICAL MODEL

We can now write down the complete set of equations describing the evolution of a collection of vortices, under the assumption that the contours of each vortex remain nearly elliptical and do not cross. Let the subscripts α and β specify distinct vortices, the subscripts j and l the contours within a vortex, and m the disturbance symmetry. Let vortex α have N_α contours, and let there be S vortices altogether.

With appropriate notation, the final expressions can be put in a compact form. Define

$$q_{kl\beta j\alpha} \equiv \exp(-\breve{w}_{kl\beta j\alpha})$$

and

$$\Sigma_{mj\alpha} \equiv \frac{1}{\nu_{j\alpha}^m} \sum_{\substack{\beta=1 \\ \beta\neq\alpha}}^{S} \sum_{l=1}^{N_\beta} \kappa_{l\beta} \sum_{k=1}^{K} \mu_k q_{kl\beta j\alpha}^m.$$

Here, $q_{kl\beta j\alpha}$, or q_k for short, is determined as the smallest root (in modulus) of the quadratic equation

$$q_k^2 - 2\frac{Z_{l\beta} + 2s_k\nu_{l\beta} - Z_{j\alpha}}{2\nu_{j\alpha}} q_k + 1 = 0.$$

The μ_k and s_k are the dimensionless strengths and positions of the point vortices used in the separated contour computations [see Part I, Eqs. (34) and (35)].

Next, define

$$\Omega_{j\alpha} \equiv \tfrac{1}{2}\omega_{j\alpha},$$
$$\Omega_{ej\alpha} \equiv \omega_{j\alpha}\lambda_{j\alpha}/(1+\lambda_{j\alpha})^2,$$
$$\gamma_{j\alpha} \equiv \tfrac{1}{2}\omega_{j\alpha}\epsilon_{j\alpha}^2 e^{-2i\phi_{j\alpha}},$$
$$\gamma_s \equiv \gamma e^{-2i\phi_s},$$
$$Z_{jl\alpha} \equiv Z_{j\alpha} - Z_{l\alpha},$$
$$\Xi_{j\alpha} \equiv \gamma_{j\alpha} \sum_{l=1}^{j-1} \frac{\kappa_{l\alpha}}{\kappa_{j\alpha}} \left\{ 1 - \left(\frac{\nu_{l\alpha}}{\nu_{j\alpha}}\right)^2 - \left(\frac{Z_{jl\alpha}}{\nu_{j\alpha}}\right)^2 \right\},$$
$$\Omega_{j\alpha}^0 \equiv \Omega + \Omega_{ej\alpha} \sum_{l=1}^{j-1} \frac{\kappa_{l\alpha}}{\kappa_{j\alpha}} + \epsilon_{j\alpha}^{-2} \Re\left[\Xi_{j\alpha} e^{2i\phi_{j\alpha}}\right] + \frac{1}{2}\sum_{l=j}^{N_\alpha} \omega_{l\alpha},$$
$$\gamma_{j\alpha}^0 \equiv \gamma_s + \Xi_{j\alpha} + \sum_{l=j}^{N_\alpha} \gamma_{l\alpha} + \Sigma_{2j\alpha}.$$

Then, the basic-state equations take the form

$$\dot{Z}_{j\alpha} = i\sum_{l=1}^{j-1} \frac{\kappa_{l\alpha}}{\kappa_{j\alpha}} (\Omega_{j\alpha} Z_{jl\alpha} - \gamma_{j\alpha}^* Z_{jl\alpha}^*) + i\sum_{l=j}^{N_\alpha} (\Omega_{l\alpha} Z_{jl\alpha} - \gamma_{l\alpha}^* Z_{jl\alpha}^*) + i(\Omega Z_{j\alpha} - \gamma_s^* Z_{j\alpha}^* - \Sigma_{1j\alpha}^*), \tag{25a}$$

$$\dot{\lambda}_{j\alpha} = 2\lambda_{j\alpha}\Im\left[\gamma_{j\alpha}^0 e^{2i\phi_{j\alpha}}\right], \tag{25b}$$

$$\dot{\phi}_{j\alpha} = \Omega_{j\alpha}^0 - \frac{1+\lambda_{j\alpha}^2}{1-\lambda_{j\alpha}^2}\Re\left[\gamma_{j\alpha}^0 e^{2i\phi_{j\alpha}}\right]. \tag{25c}$$

The last two equations are identical to those derived by Kida[4] for a single elliptical patch upon suppressing all subscripts and superscripts. Therefore, $\gamma_{j\alpha}^0$ and $\Omega_{j\alpha}^0$ can be thought of as generalized strain and background rotation rates.

The disturbance equations are simplified by introducing a few more definitions:

$$\mathscr{A}_{mj\alpha} \equiv (A_{mj\alpha} + iB_{mj\alpha}) e^{im\phi_{j\alpha}},$$
$$\tilde{\Omega}_{j\alpha} \equiv \bar{\Omega}_{j\alpha} + \dot{\phi}_{j\alpha},$$
$$= \Omega + 2\Omega_{ej\alpha}\sum_{l=1}^{j-1}\frac{\kappa_{l\alpha}}{\kappa_{j\alpha}} + \frac{1}{2}\sum_{l=j}^{N_\alpha}\omega_{l\alpha} - \epsilon_{j\alpha}^2\,\Re\left[\gamma_{j\alpha}^0 e^{2i\phi_{j\alpha}}\right],$$
$$r_{+j\alpha} \equiv \tfrac{1}{2}(a_{j\alpha} \pm b_{j\alpha}).$$

Then, we find

$$\dot{\mathscr{A}}_{mj\alpha} = im\tilde{\Omega}_{j\alpha}\mathscr{A}_{mj\alpha} - i\left(\frac{\nu_{j\alpha}}{r_{+j\alpha}}\right)^m \sum_{l=1}^{j-1} \kappa_{l\alpha} G_m\left(\frac{\nu_{l\alpha}}{\nu_{j\alpha}}, \frac{Z_{lj\alpha}}{\nu_{j\alpha}}\right) - \frac{1}{2} i r_{+j\alpha}^m \left\{ \Sigma_{mj\alpha}^* + \left(\frac{\nu_{j\alpha}^*}{r_{+j\alpha}}\right)^{2m} \Sigma_{mj\alpha} \right\}$$
$$- \frac{1}{2} i \sum_{l=1}^{j-1} \omega_{l\alpha} \left\{ \left(\frac{r_{+l\alpha}}{r_{+j\alpha}}\right)^m \mathscr{A}_{ml\alpha} + \left(\frac{r_{-l\alpha}}{r_{+j\alpha}}\right)^m \mathscr{A}_{ml\alpha}^* e^{2im\phi_{j\alpha}} \right\}$$
$$- \frac{1}{2} i \sum_{l=j}^{N_\alpha} \omega_{l\alpha} \left\{ \left(\frac{r_{+j\alpha}}{r_{+l\alpha}}\right)^m \mathscr{A}_{ml\alpha} + \left(\frac{r_{-j\alpha}}{r_{+l\alpha}}\right)^m \mathscr{A}_{ml\alpha}^* e^{2im\phi_{j\alpha}} \right\}. \tag{25d}$$

The coefficients G_m are given in Appendix B. The second and third terms recover the nonelliptical part of the velocity field produced by the basic ellipses.

VII. THE MODEL EQUATIONS IN A FEW SPECIAL CASES

Theoretically intriguing sets of equations arise in several problems of fundamental interest. Consider first the equations for two nested contours without a common center. Let the index "1" refer to the interior contour and "2" to the exterior contour. In the absence of an external straining flow, the centroids evolve according to

$$\dot{Z}_1 = \tfrac{1}{2} i\omega_2 (Z_{12} - \epsilon_2^2 Z_{12}^* e^{2i\phi_2}), \tag{26a}$$

$$\dot{Z}_2 = \tfrac{1}{2} i\omega_2 (\kappa_1/\kappa_2)(Z_{21} - \epsilon_2^2 Z_{21}^* e^{2i\phi_2}) \tag{26b}$$

or

$$\dot{Z}_{21} = \tfrac{1}{2} i\omega_2(\kappa_1/\kappa_2 + 1)(Z_{21} - \epsilon_2^2 Z_{21}^* e^{2i\phi_2}), \tag{26c}$$

$$\kappa_1 \dot{Z}_1 + \kappa_2 \dot{Z}_2 = 0, \tag{26d}$$

the last equation expressing conservation of linear momentum. Let $Z_{21} = Re^{i\theta}$. Then, for the aspect ratios,

$$\frac{\dot{\lambda}_1}{\lambda_1} = \omega_2 \epsilon_2^2 \sin 2\phi_{12}, \tag{27a}$$

$$\frac{\dot{\lambda}_2}{\lambda_2} = \omega_2 \epsilon_2^2 \frac{\kappa_1}{\kappa_2}\left\{\left(\frac{c_1}{c_2}\right)^2 \sin 2\phi_{21} + \left(\frac{2R}{c_2}\right)^2 \sin 2(\phi_2 - \theta)\right\}. \tag{27b}$$

Here, one can verify $\kappa_1 c_1^2 \dot{\lambda}_1/\lambda_1 + \kappa_2 c_2^2 \dot{\lambda}_2/\lambda_2 + 8R\dot{R}\kappa_1\kappa_2/(\kappa_1 + \kappa_2) = 0$ — this is a consequence of angular momentum conservation. And, for the orientations,

$$\dot{\phi}_1 = \Omega_{e1} + \frac{1}{2}\omega_2\left(1 - \frac{1+\lambda_1^2}{1-\lambda_1^2}\epsilon_2^2 \cos 2\phi_{12}\right), \tag{28a}$$

$$\dot{\phi}_2 = \Omega_{e2} + \Omega_{e2}\frac{\kappa_1}{\kappa_2}\left\{2 - \left(\frac{c_1}{c_2}\right)^2 \cos 2\phi_{21} - \left(\frac{2R}{c_2}\right)^2 \cos 2(\phi_2 - \theta)\right\}. \tag{28b}$$

Conservation of energy (see Part I, Sec. VII) further reduces the number of independent variables to four. In addition, these equations only depend on the angular differences $\phi_2 - \phi_1$ and $\phi_2 - \theta$, so that just three independent variables remain. As such, this system may be an interesting one to explore chaotic vortex motion.

A second system leading to three independent variables is found in the motion of two symmetrical vortices in a uniform external straining flow. Each vortex, a single contour, has identical vorticity ω, circulation κ, aspect ratio λ, and orientation ϕ, but opposite centroids (at Z and $-Z$). In this case, the centroid of one vortex evolves according to

$$\dot{Z} = i(\Omega Z - \gamma Z^* - \Sigma_1^*), \tag{29}$$

where $\Sigma_m = \kappa \nu^{-m} \Sigma_{k=1}^K \mu_k q_k^m$, $\nu = \frac{1}{2} ce^{i\phi}$, and each q_k is determined as the smallest magnitude root of

$$q_k^2 - 2(s_k - Z/\nu)q_k + 1 = 0;$$

in addition,

$$\dot{\lambda} = 2\lambda(\gamma \sin 2\phi + \Im[\Sigma_2 e^{2i\phi}]), \tag{30}$$

and

$$\dot{\phi} = \Omega_e + \Omega - \frac{1+\lambda^2}{1-\lambda^2}(\gamma \cos 2\phi + \Re[\Sigma_2 e^{2i\phi}]). \tag{31}$$

There are therefore four real variables. Conservation of angular momentum is violated by the external straining flow, but conservation of energy still holds, provided one takes into account an interaction energy between the straining flow and the vortices (see Part I, Sec. VII and Ref. 3, Appendix). So, there are only three independent variables in this system. (*Note*: strict conservation of the invariants can only be obtained if we approximate the advectee in the same way as the advector, that is by an equivalent number of point vortices. This leads to a different expression for the Σ_m terms—see Part I, Secs. VI and VII for further discussion.)

VIII. MODEL TESTS

This section presents comparisons between the elliptical model (hereafter EM) and the full (contour dynamics) equations of motion (CD) in a few simple cases. Comparisons are also made with the moment model (MM) of Ref. 5, where possible. Four topics are examined: (1) the equilibrium contour shapes of a multicontour family of vortices in uniform strain; (2) the linear stability of this family; (3) the equilibrium boundary shapes of two identical corotating patches; and (4) the time evolution of two symmetrical, unsteady patches, including merging.

A. Equilibrium contour shapes of a multicontour vortex in strain

We specify the vorticity distribution by the area enclosed by each contour, $\pi R_j^2, j = 1,2,...,N$, and the vorticity jump across each contour, ω_j. The vortex is subjected to an external straining flow characterized by $\gamma = 6/65$ and $\Omega = 0$. The results below are obtained with $N = 8$ contours and with all the ω_j equal to $1/N$. We choose the areas within the contours to correspond to the vorticity profile used by Melander *et al.*[6] (see Ref. 7 for details, including the numerical method used to obtain the CD results). It is sufficient here to note that the πR_j^2 depend parametrically on a quantity δ, such that when $\delta = 0$, all of the contours lie on top of one another (and the equilibrium shape is then an ellipse of aspect ratio 2/3 for the value of γ given above[8]), and when $\delta = 1$, the contours are most distinct (the corresponding vorticity profile then resembles a Gaussian).

The EM results are calculated by solving the set of simultaneous nonlinear equations, $\phi_j = 0$ (with $\phi_j = 0$), for the $\lambda_j, j = 1,...,N$ ($N = 8$). This is done by using the known solution at $\delta = 0$ as a first guess in an iterative Newton method for the solution at $\delta = 0.01$. Solutions for greater values of δ are generated in the same way, using previous solutions as first guesses. Disturbances can be included later by solving $\mathscr{A}_{mj} = 0$ for the $\mathscr{A}_{mj}$. But, by symmetry, only cosinusoidal disturbances with even wave numbers m will be excited (so $B_{mj} = 0$). The A_{mj}, for even m, are determined from the special form of (25d) applying here,

$$m\tilde{\Omega}_j A_{mj} = \frac{1}{2}\omega\left(\frac{c_j}{r_{+j}}\right)^m \sum_{l=1}^{j-1} R_l^2 G_m\left(\frac{c_l}{c_j}, 0\right) + \frac{1}{2}\omega \sum_{l=1}^{j-1} \frac{r_{+j}^m + r_{-j}^m}{r_{+l}^m} A_{ml} + \frac{1}{2}\omega \sum_{l=j}^{N} \frac{r_{+l}^m + r_{-l}^m}{r_{+j}^m} A_{ml}, \tag{32}$$

where $\omega = 1/N$, and $\tilde{\Omega}_j$ is defined in Sec. VI. Wave numbers $m = 4$, 6, 8, and 10 are included in the following results.

Figures 2(a) and 2(b) show the equilibrium contour shapes for $\delta = 0.5$ and $\delta = 0.98$; the three curves correspond to CD (solid), EM (basic model only; dashed), and EM (full model; dotted). (The MM is inapplicable in this case since it cannot handle embedded contours.) At $\delta = 0.5$, the close spacing of the contours results in very close agreement between all of the results. Quantitatively, the *full* EM gives the best agreement; for example the x intercept of the outer-

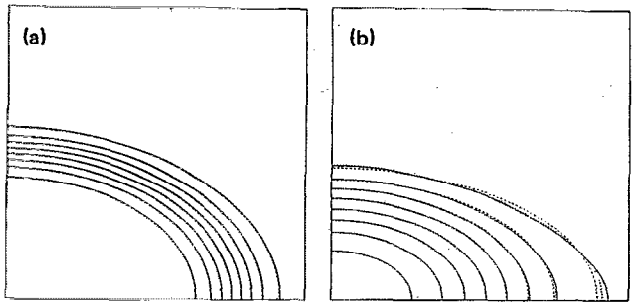

FIG. 2. A comparison of CD, basic EM, and full EM nested equilibria (solid, dashed, and dotted lines, respectively) for two values of the profile steepness: (a) $\delta = 0.5$ and (b) $\delta = 0.98$. Only one quadrant of the vortex is shown—the rest is mirror symmetric about the x and y axes.

most contour is $x = 1.101\ 24$ for CD, $x = 1.100\ 60$ for the full EM, and $x = 1.097\ 36$ for the basic EM. At $\delta = 0.98$, the maximum value of δ for which the iterative scheme used to calculate the EM equilibria could be made to converge (owing to the presence of nearby external stagnation points), the agreement is poorer, although the inclusion of disturbances within the EM again leads to significant improvements. The remaining differences between the full EM and CD must be due to the neglected disturbance coupling with the basic flow and with disturbances having different symmetries (as discussed in Sec. IV), as well as neglected nonlinearity.

B. Linear stability of a multicontour vortex in strain

The equilibria just examined are next subjected to small disturbances. The linear stability results for CD were obtained numerically using a highly accurate matrix method (see Ref. 9 for details). In this method, the disturbance on each contour is represented by a 32-term series in $\cos m\vartheta$ and $\sin m\vartheta$, where ϑ is a coordinate proportional to the travel time of a fluid particle from a fixed position around an undisturbed contour. The computed eigenvalues change by less than one part in 10^5 upon doubling the number of terms from 32 to 64. The EM results were obtained by substituting $\mathscr{A}_{mj} = \bar{\mathscr{A}}_{mj} + \hat{\mathscr{A}}_{mj} e^{i\sigma t}$ into (25d) and finding the eigenvalues of a complex matrix of size 8×8 (this matrix is one thousand times smaller than the matrix used to obtain the CD results, owing to symmetry decoupling within the EM). Here, the $\bar{\mathscr{A}}_{mj}$ refer to the equilibrium values computed in Sec. VIII A above.

The results are compared in Fig. 3. Strictly, it is only possible to identify the bands of modes corresponding to each "pure" symmetry m in the EM, since each eigenfunction depends on just one m value. Each band is characterized by $N-1$ $(=7)$ "internal" neutral modes having "critical levels" between successive pairs of contours, and one "external" mode having a critical level beyond the vortex edge. In the figure, the internal modes can be seen to be stemming from the same source when $\delta = 0$ and spreading out gradually as δ is increased. The external mode takes a significantly different route as δ is increased. Comparing the results, we see small discrepancies only when δ approaches unity, when

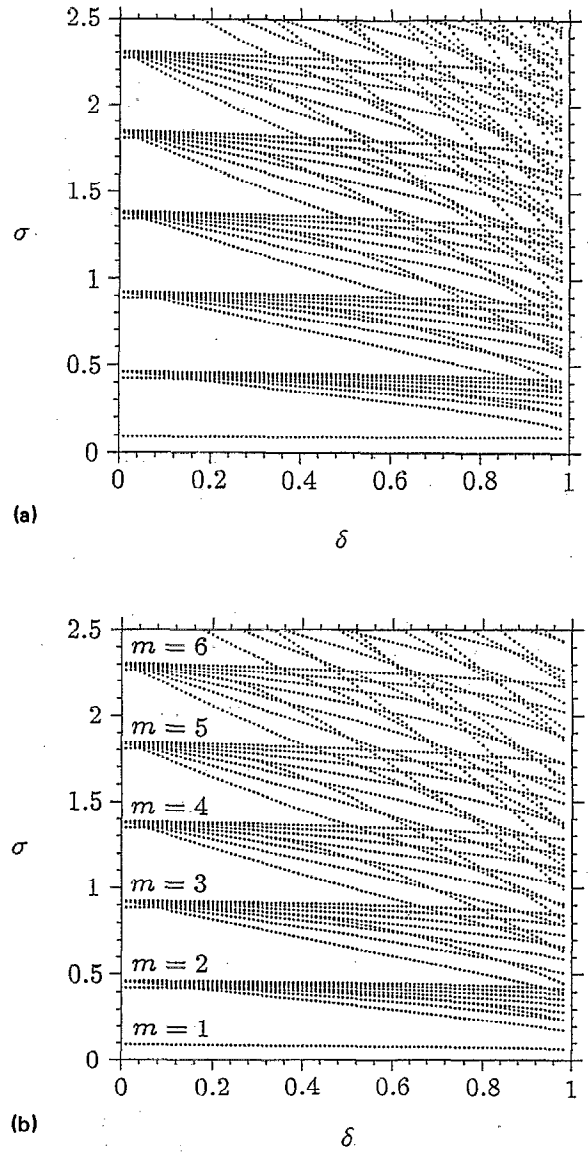

FIG. 3. A plot showing the eigenvalues σ as a function of the width of the vortex edge, proportional to δ, for a particular family of distributed-vorticity equilibria; (a) as computed using CD, and (b) as computed using the EM. All of the eigenvalues shown are real, implying neutral stability, except those of the lowest curve, labeled $m = 1$ in (b) for which we plot only the real part. The instability of the $m = 1$ mode reflects the fact that a small initial displacement in the vortex centroid can be compounded by the external strain. Other $m = 1$ modes lie along the line $\sigma = 0$, and the whole diagram is mirror symmetric across this line.

the demands on the EM are greatest. Given the complexity of the linear stability diagram, the overall agreement between the EM and CD results is not insignificant.

C. Equilibrium contour shapes for a pair of identical corotating vortex patches

The problem of finding corotating equilibria was first examined by Saffman and Szeto[10] and later reexamined and extended to more than two vortices by Dritschel.[11] Each vortex has unit vorticity and possesses twofold symmetry. The closest distance between one vortex and the origin about

which it rotates is given by a_0, and the distance to the farthest point on its boundary from the origin is unity (see Fig. 4). The problem is to determine the boundary shape of half of one vortex and the background rotation $\Omega = -\Omega_0$ that keeps the vortices stationary. Using CD, this problem is tackled using a nonlinear iterative scheme. The results presented below use the method described in Ref. 11, with a numerical resolution sufficiently fine to make Ω_0 accurate to six figures.

Using the EM, with disturbances, we specify the distance between centroids r, assuming each patch has area equal to π, and calculate the basic-state aspect ratio λ and steady rotation $\Omega = -\Omega_0$ from the conditions $\dot{Y} = 0$, or no centroid movement, and $\dot{\phi} = 0$, or no vortex rotation ($\dot{X}$ and $\dot{\lambda}$ are automatically zero on geometrical grounds—see Fig. 4). We then calculate $\bar{\Omega}$ and the disturbance amplitudes A_m, the latter from the condition $\dot{B}_m = 0$ (again $\dot{A}_m = 0 = B_m$ automatically). From this, we can obtain the boundary shape, inclusive of nonelliptical deformations. For comparisons, we search for the EM equilibrium with the dimensionless ratio of angular momentum to squared area equal to that of the CD equilibrium, and then shrink the EM equilibrium until it has the same area as the CD equilibrium.

In detail, the procedure is as follows. Each vortex has $\omega = R = 1$ and thus $\kappa = 1/2$. Referring to Fig. 4, let the left-hand vortex be the advectee. Then the condition of no centroid movement is

$$\dot{Y} = \frac{1}{2}\Omega_0 r - \frac{1}{c}\sum_{k=1}^{K}\mu_k q_k = 0, \tag{33}$$

where $q_k = r/c + s_k - \{(r/c + s_k)^2 - 1\}^{1/2}$, while the condition of no vortex rotation is

$$\dot{\phi} = \Omega_e - \Omega_0 - \frac{1}{c^2}(\epsilon^{-2} + \epsilon^2)\sum_{k=1}^{K}\mu_k q_k^2 = 0. \tag{34}$$

The simultaneous solution of these equations gives $\lambda(r)$ and $\Omega_0(r)$ (a simple interval-dividing method is used, with accuracy to better than ten significant figures). Given λ and $\Omega_0(r)$, the disturbance quantities are readily computed. Here, $\bar{\Omega}$ is given by

$$\bar{\Omega} = \Omega_e + \frac{1}{c^2}(\epsilon^{-2} - \epsilon^2)\sum_{k=1}^{K}\mu_k q_k^2, \tag{35}$$

and the A_m, $m = 3,4,\ldots$ are determined from

$$\dot{B}_m = 0 = \left\{m\bar{\Omega} - \frac{1}{2}(1 + \epsilon^{2m})\right\}A_m - \frac{1}{2}(\epsilon^{-m} + \epsilon^m)\sum_{k=1}^{K}\mu_k q_k^m. \tag{36}$$

We used $K = 10$ and calculated A_m up to $m = 20$ to obtain a minimum accuracy of six significant figures in the boundary shape.

Figure 5 compares the boundary shape determined using CD (dashed contour) with that determined from the EM (solid contour) for three values of a_0 corresponding to a small separation between the vortices: $a_0 = 0.3$ (top), $a_0 = 0.2$ (middle), and $a_0 = 0.1$ (bottom). The percentage errors in the rotation rate Ω_0 for these values of a_0 are 0.054, 0.25, and 1.2, respectively. Again, we find surprisingly high accuracy for the elliptical model.

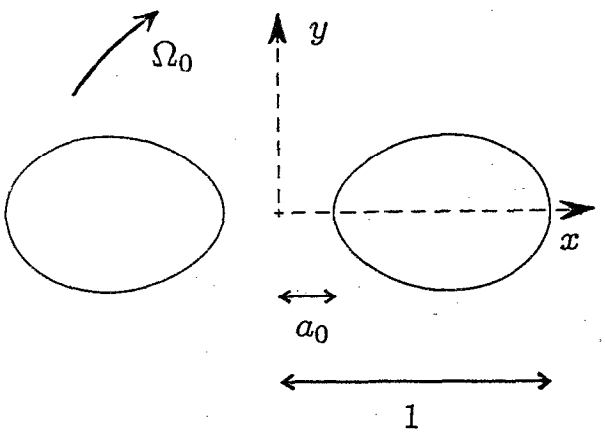

FIG. 4. Equilibrium configuration of two corotating vortices.

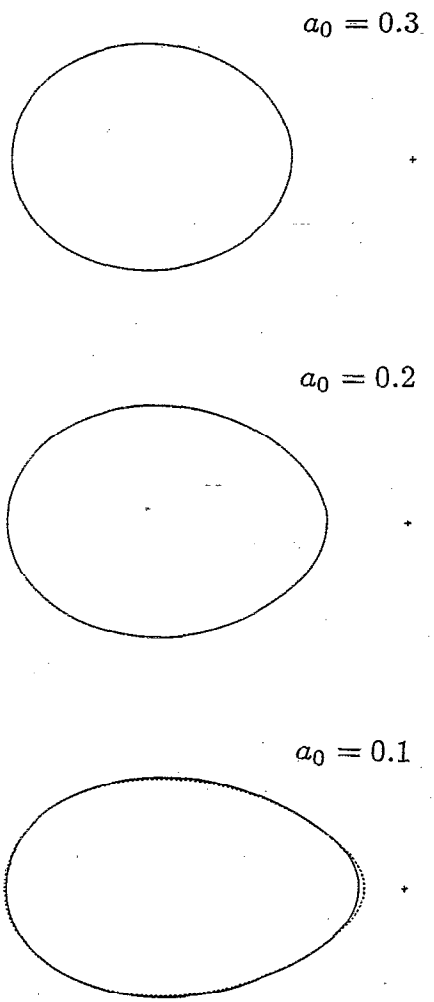

FIG. 5. The boundary shapes of one of a pair of identical corotating vortices for three close separation distances. The dashed lines were computed by CD, and the solid lines from the EM. The plus sign marks the center of rotation.

D. Unsteady, symmetric vortex patch evolution

We next attempt to follow the evolution of interacting vortices using the EM. The governing model equations are given by (30) and (31), for the basic evolution, and the specialized form of (25d), for the disturbance evolution. No external straining flow is assumed to be present ($\gamma = \Omega = 0$). We begin with two precisely circular vortices (with unit vorticity and radius) separated by a distance d from center to center. This is the now well-studied problem of symmetric vortex merger going back to Zabusky *et al.*[12] On the basis of CD calculations, the vortices merge only if $d < 3.4$. Here we examine the two cases $d = 4$ and $d = 3$.

The EM results are compared with CD simulations done at sufficiently high resolution to ensure that the plotted results are accurate to within the plotted linewidth (see Ref. 13) for support; the algorithm parameters used in the calculations presented are $\mu = 0.03$ and $\Delta t = 0.05$). The EM equations are solved by combining (30) and (31) into a single equation for the complex variable $\frac{1}{2} c^2 e^{-2i\phi}$. The advantage of this is that the resulting equation does not have singular coefficients when $\lambda = 1$. Here, $K = 5$ point vortices are used to represent the flow field of the advector, although $K = 1$ was also used to verify that $K = 5$ gives significantly better results (larger values of K, on the other hand, do not lead to noticeable improvements). (It was pointed out in Sec. V that these equations do not strictly conserve the invariants of motion unless a further approximation is made, yet, in the first numerical simulation shown below, the angular momentum changes by only one part in 10^{10}; in the second, it changes by one part in 10^4.) A fourth-order Runge–Kutta scheme was used for the time integration, with time step $\Delta t = \pi/80$. A similar numerical code was written to solve the moment model (MM) equations[14] to enable comparisons between the two approximate models.

Figure 6(a) for $d = 4$ compares the evolution computed by CD (solid contours) with that computed by the EM *without* disturbances (dashed contours), and Fig. 6(b) shows the improvement one gets by including disturbances in the model. See also Fig. 6(c)for a close-up view at $t = 4.5$, including a comparison with the MM. The full EM is virtually indistinguishable from CD in this example. Even without disturbances, the EM does better than the MM—the quantitative results given in Table I indicate at least a threefold improvement in this case and in another for $d = 3.5$.

Figure 7(a), for $d = 3$, shows vortex merger computed using CD. Figures 7(b), 7(c), and 7(d) show the corresponding model results, obtained with the MM, the basic EM, and the full EM, respectively. Here, the assumptions underpinning both models eventually break down as the vortices merge, since both models require that the elliptical focal separation $2c$ be small compared to the distance between the vortex centroids. Nevertheless, the full EM does capture the early stages of merging, including substantial nonelliptical deformations.

The results obtained with the basic model are interesting in their own right. In particular, the criterion for "merging" in the EM is qualitatively the same one observed in CD. Arguably, the same similarity exists between the MM and CD. However, there is an apparent difference between the two approximate models: the EM exhibits periodic, recursive behavior while the MM exhibits centroid collapse in finite time (this is noted in Ref. 14). Both behaviors are consistent with an integrable two-degree-of-freedom system. Centroid collapse within the MM is interpreted as merging by Ref. 14, and on this basis, the MM predicts merging when $d < 3.2$ (recall that the result for contour dynamics is $d < 3.4$). The EM, on the other hand, never exhibits centroid collapse for any admissible value of the initial centroid separation d. Something else occurs. Compare Figs. 8(a) and 8(b), for two calculations beginning with slightly different centroid separations, $d = 3.35$ and 3.351, respectively. After $t = 4$, the two solutions bifurcate, in one case the vortices become more elongated and in the other they begin returning to their initially circular shape. Note that the bifurcation is characterized by a reversal in relative phase rotation, $\Delta\Omega \equiv \dot{\phi} - \dot{\theta}$, with θ defined by $Z = Re^{i\theta}$. That is, for $d = 3.351$ [Fig. 8(b)], $\Delta\Omega$ remains positive throughout the evolution, whereas for $d = 3.35$, $\Delta\Omega$ reverses sign around $t = 4$. There is a critical value of d, near 3.350 275, for which the vortices settle into a steadily rotating configuration, but an apparently unstable one. [In the context of the D–G diagram presented in Ref. 14 (effectively a plot of the excess energy $\mathscr{H}$ as a function of the real and the imaginary parts of $c^2 e^{2i(\phi - \theta)}$, for fixed angular impulse $\mathscr{I}$), merging is a consequence of the existence of a saddle point in this diagram, *not* of centroid collapse. It just so happens that a saddle point allows solution trajectories to turn toward a finite time singularity in the MM.] Now consider the CD simulations. Figure 6(b) for $d = 4$ shows that $\Delta\Omega > 0$ throughout the evolution, and the vortices do not merge. Figure 7(a) for $d = 3$ shows that $\Delta\Omega < 0$ immediately before merging. An extensive series of CD simulations closer to the critical merging distance (see Waugh[15]) confirms that nonmerging cases are all accompanied by $\Delta\Omega > 0$, while merging cases are accompanied by $\Delta\Omega < 0$ at some stage before merging. Between these cases, in the range $3.31 < d < 3.43$, the vortices partly merge and then break apart again, sometimes repeating this several times. In this range, the time dependence of $\Delta\Omega$ is more complicated (see Ref. 15 for details). The conclusion is that the appearance of negative $\Delta\Omega$ occurs in CD, in the EM, *and* in the MM, and it indicates merging. Furthermore, of the two approximate models, the EM gives the most accurate criterion for merging, in terms of critical initial separation distance.

IX. DISCUSSION

By representing vortices as stacks of nested patches of uniform vorticity, each patch being nearly elliptical, we have arrived at an approximate set of equations both radically different from and vastly less expensive to solve than the full contour dynamics equations. These approximate equations should afford many simple investigations of fluid motion in two dimensions and should make possible some investigations which are at present too costly for full contour dynamics simulations.

We have arrived at the model equations on the primary assumption that contours within vortices remain very nearly elliptical in the velocity field induced by the same and other

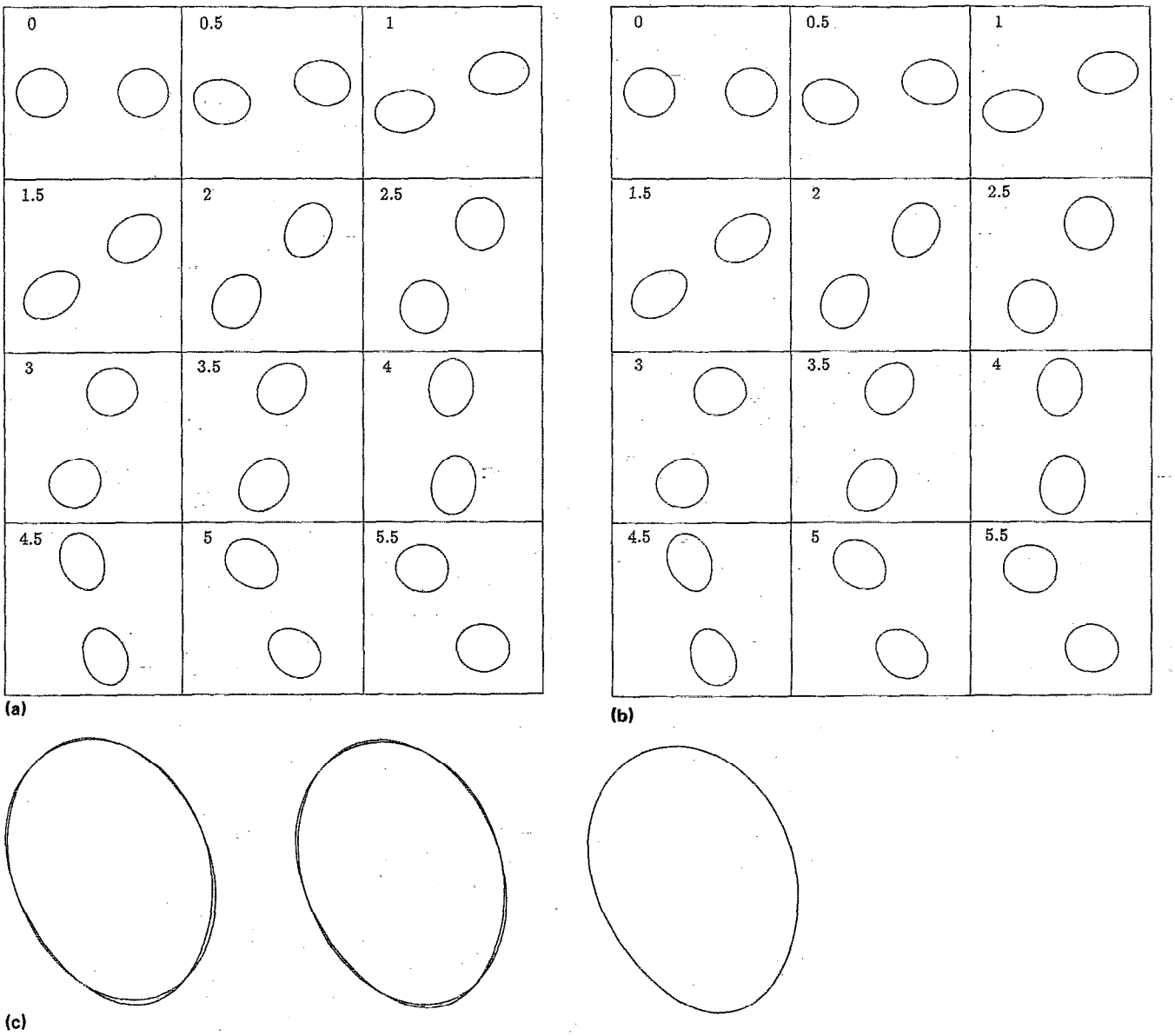

FIG. 6. (a) A comparison of a CD simulation (solid lines) and a basic EM simulation (dashed lines) for two initially circular vortices separated by four vortex radii from center to center. Time (in units of $2\pi/\omega$) proceeds to the right and downwards. (b) Same as in (a) except the full EM is used. (c) Comparisons at $t = 4.5$ between CD and the MM (left), between CD and the basic EM (middle), and between CD and the full EM (right).

TABLE I. Quantitative comparisons between the MM, the EM, and CD in two examples of unsteady vortex patch evolution.[a]

	MM	Basic EM	CD
	Comparison at $t = 4.5$ for patches initially $d = 4$ radii apart		
Z	$-0.443\,946 + 1.942\,997i$	$-0.447\,340 + 1.941\,651i$	$-0.449\,050 + 1.941\,036i$
$ce^{i\phi}$	$-0.295\,782 + 0.766\,209i$	$-0.289\,757 + 0.785\,946i$	$-0.286\,895 + 0.787\,164i$
% error in Z	0.274	0.091	...
% error in $ce^{i\phi}$	2.72	0.371	...
	Comparison at $t = 5.5$ for patches initially $d = 3.5$ radii apart		
Z	$-1.691\,889 + 0.359\,295i$	$-1.692\,596 + 0.325\,498i$	$-1.693\,776 + 0.310\,503i$
$ce^{i\phi}$	$-1.044\,001 + 0.111\,396i$	$-1.104\,705 + 0.212\,129i$	$-1.097\,812 + 0.252\,770i$
% error in Z	2.84	0.87	...
% error in $ce^{i\phi}$	13.4	3.66	...

[a] *Note*: The percent error in a complex quantity Q is defined as $100|Q_{\text{model}} - Q_{\text{CD}}|/|Q_{\text{CD}}|$. The elliptical parameters were extracted from the CD simulation by computing the second moments of one vortex, defined by $\int\int \omega x^2$, $\int\int \omega y^2$, and $\int\int \omega xy$, relative to the centroid of that vortex, and finding the ellipse with the same second moments.

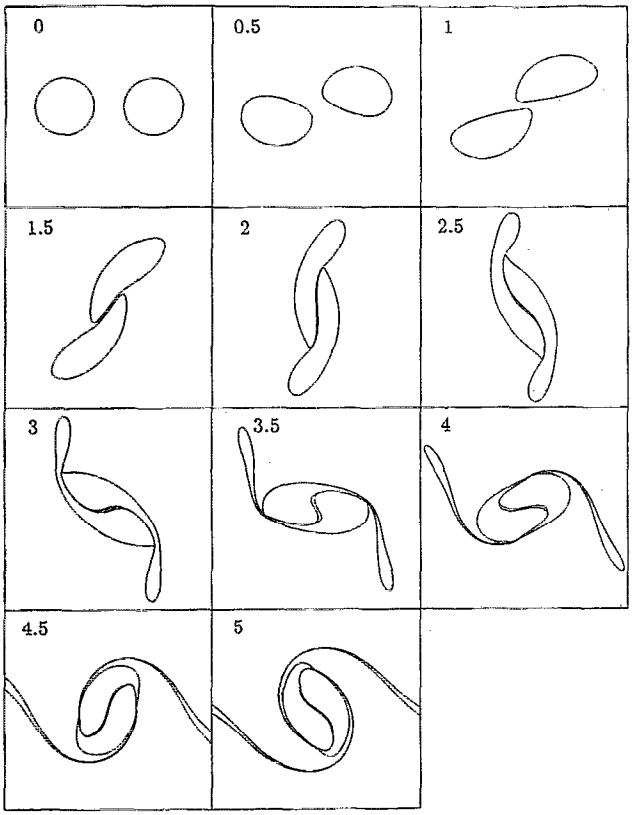

(a)

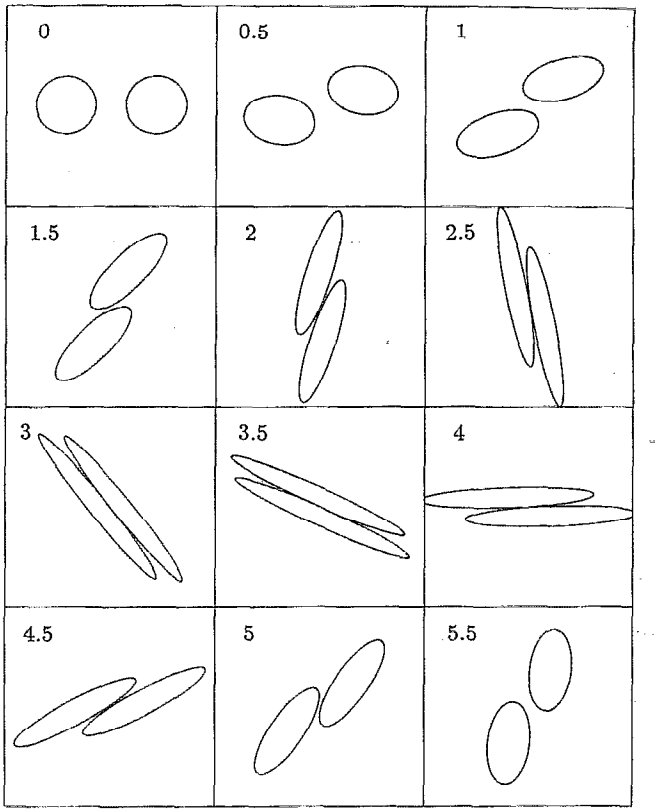

(c)

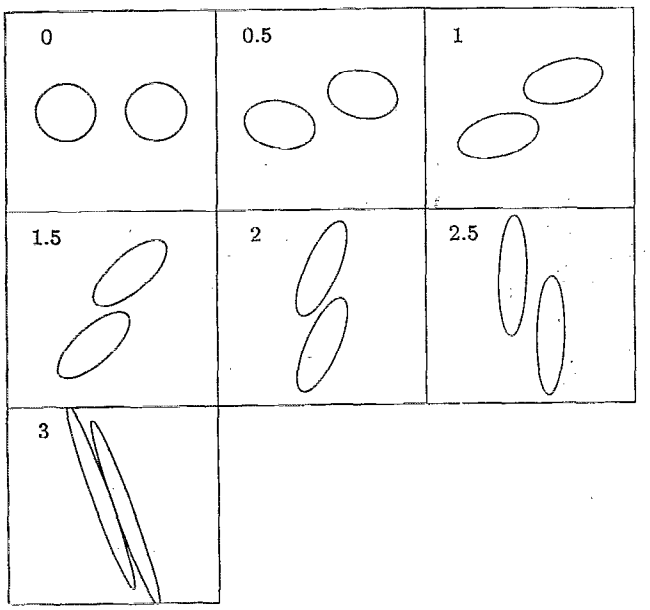

(b)

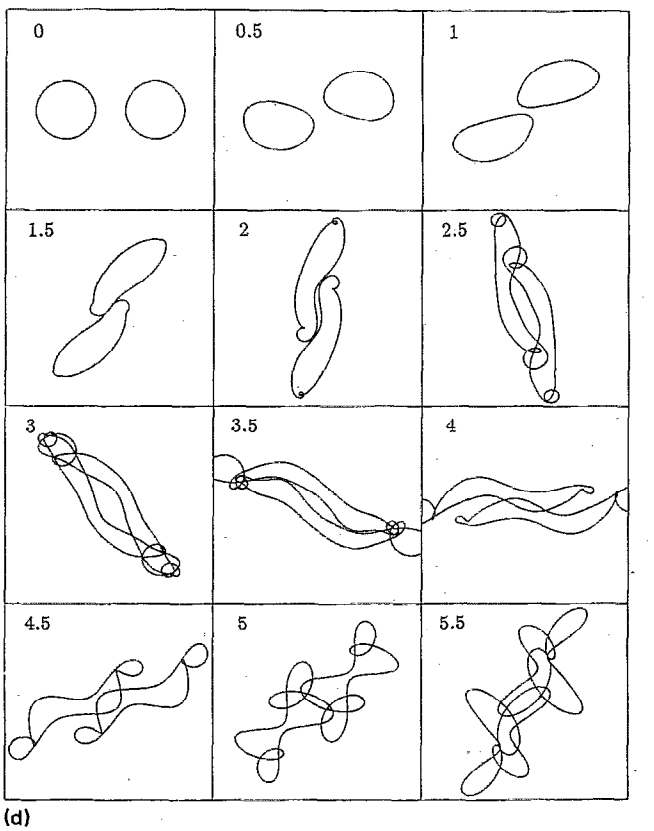

(d)

FIG. 7. (a) A CD simulation of vortex merger starting from initially circular vortices separated by three vortex radii. (b) The corresponding MM simulation. (c) The basic EM simulation. (d) The full EM simulation.

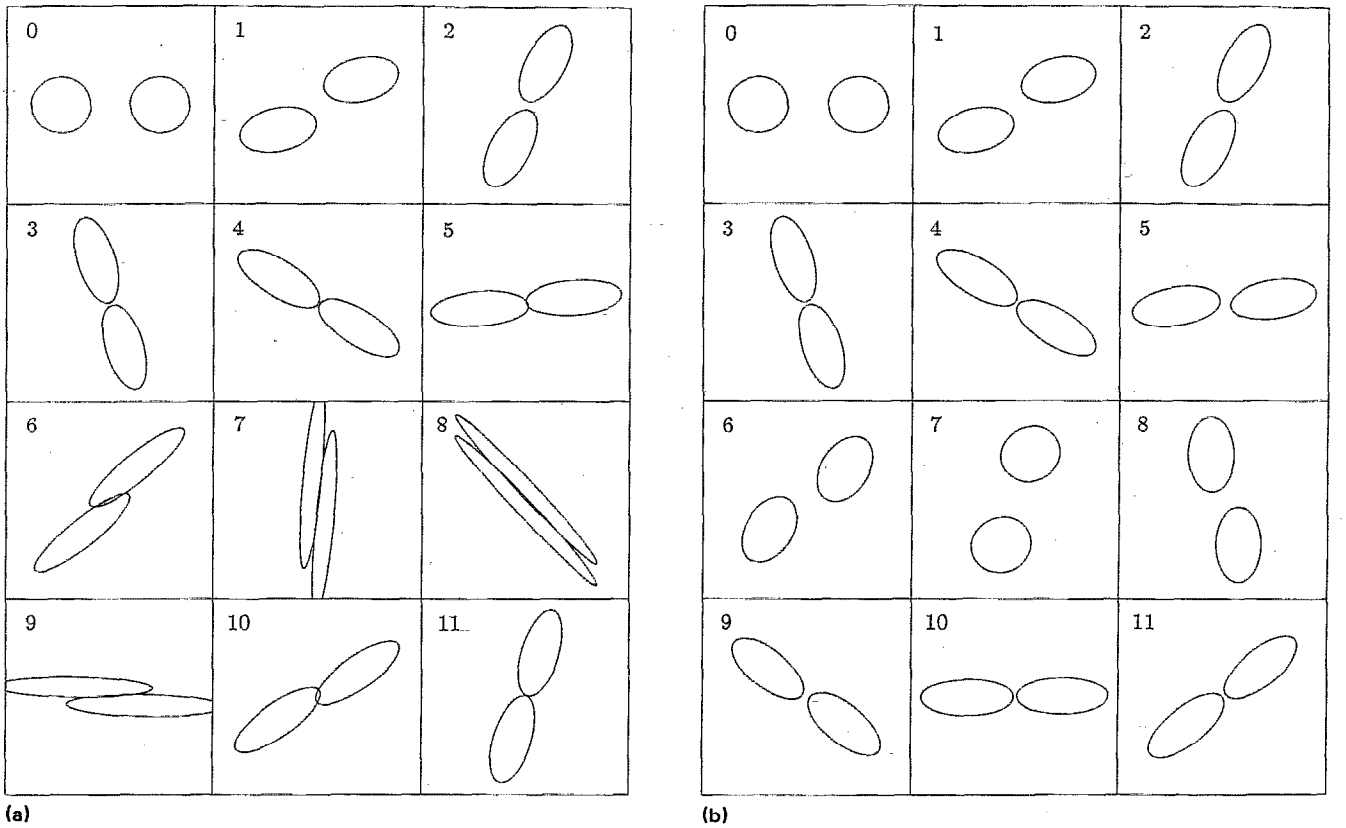

FIG. 8. (a) An EM (basic) simulation beginning with two circular vortices 3.35 radii apart. (b) Same as in (a) except the vortices are 3.351 radii apart initially.

contours. In the basic model, all contours evolve under the constraint that they remain precisely elliptical, so a part of the velocity field set up by these ellipses is discarded. In the disturbance model, this discarded part of the velocity field is used to generate disturbances. Nonlinear effects such as cascading and feedback on the basic flow are not retained (the full model is thus non-Hamiltonian).

It is noteworthy that we have not from the outset expanded in some small parameter or parameters to obtain our model set of equations by perturbation theory. Instead, we have performed a Galerkin expansion, using the centroid and the elliptical parameters as our expansion "functions." This has nevertheless yielded a self-consistent model, one which appears to be significantly more accurate in fact than the moment model, judging by the comparisons shown in Sec. VIII. (Perhaps this is not surprising since the moment model can be obtained as an approximation of the elliptical model—see Part I, Sec. VI.) Ultimately, the validity and utility of the elliptical model must rest on its comparison with contour dynamics as well as with other approximate models.

At present, work is in progress to examine vortex merger in an external straining flow, in an effort to understand the conditions for and efficiency of merger in two-dimensional vortex dynamics. A study is planned which combines contour dynamics/surgery with the elliptical model to investigate turbulence at essentially infinite Reynolds numbers, in order to obtain statistical information such as the rate of growth of vortex structures, without the usual limitations of vorticity and vorticity-gradient decay. The combined model offers the attraction of inexpensive computation over the bulk of the fluid, as only a small percentage of the vortices are expected to be engaged in the merger process at any one time. Efforts are also being made to incorporate some nonconservation effects, such as the loss of filaments through stripping[9] while remaining wholly within the basic elliptical model. Other extensions are being contemplated, including a 3-D, quasigeostrophic model to be used in studies of atmospheric and oceanic dynamics.

ACKNOWLEDGMENTS

The authors would like to thank N. J. Zabusky for his repeated encouragement. Thanks are also due to D. d'Humières for his help in determining the G_m in Appendix B by symbolic manipulation.

The contour dynamics computations were performed on the Cray X-MP/48 at Rutherford–Appleton Laboratory, with the support of the Science and Engineering Research Council and the U.S. Office of Naval Research.

APPENDIX A: DETERMINATION OF $\bar{\Omega}$

For a single elliptical vortex patch, it turns out that $\bar{\Omega}$ is independent of η, despite the forbidding appearance of (9).

This is true even in the presence of an external straining flow, when the aspect ratio and orientation generally vary with time.[3] This property greatly simplifies the linear disturbance evolution for a single elliptical patch, because it allows the modes of differing symmetries m to decouple, and only 2 ode's are necessary to describe the disturbance evolution for a given symmetry m.

For embedded ellipses within a single vortex, $\bar{\Omega}$ for each ellipse is independent of η if the ellipses are confocal. So, in general, η dependence is the result of mismatched foci. Separated ellipses also contribute η dependence. We can ignore both of these effects at the expense of introducing error, but this is justifiable since this is on the same footing as ignoring higher-order deformations within the basic model. To see why, in Part I, we have used only the $\cos 2\eta$ and $\sin 2\eta$ components of the basic-state streamfunction $\bar{\psi}(\bar{\Gamma},\eta)$ to determine the basic flow evolution. If $\bar{\Omega}$ in (9) is to be regarded as a basic-state quantity, then it can only utilize the part of the $\bar{\psi}(\bar{\Gamma},\eta)$ retained in Part I. But since $\bar{h}^2$ in (9) depends on η $[\bar{h}^2 = \frac{1}{2}(a^2+b^2) - \frac{1}{2}(a^2-b^2)\cos 2\eta]$, only the constant part of $\bar{h}^{-2}\,\partial\bar{\psi}/\partial\xi$ is strictly a basic-state quantity. Therefore, we may approximate $\bar{\Omega}$ by

$$\bar{\Omega}(t) = \frac{1}{2\pi}\int_0^{2\pi} \frac{1}{\bar{h}^2}\frac{\partial\bar{\psi}}{\partial\xi}\,d\eta - \dot{\phi}. \tag{A1}$$

There are five sources contributing to $\bar{\Omega}$ for each ellipse: (i) an external straining flow (defined below), (ii) exterior embedding ellipses, (iii) the ellipse itself, (iv) interior embedded ellipses, and (v) separated ellipses. Contribution (i) from an external straining flow is very similar to that from an exterior ellipse, so we turn to contribution (ii) first.

When the advecting elliptical vortex (Z',λ',ϕ') is exterior to the advected elliptical vortex (Z,λ,ϕ), the induced flow is given by

$$\bar{\psi}(\tilde{z}') = \tfrac{1}{8}\omega'\{2\tilde{z}'\tilde{z}'^* - \epsilon'^2(\tilde{z}'^{*2} + \tilde{z}'^2)\}, \tag{A2}$$

where $\tilde{z}'$ refers to the coordinates linked to the principal axes of the advector [see (1)]. We must change to the $\tilde{z}$ coordinate system of the advectee to determine the contribution to $\bar{\Omega}$. The two coordinate systems are related by

$$\tilde{z}' = (Z - Z')e^{-i\phi'} + \tilde{z}e^{i(\phi-\phi')}.$$

We can then evaluate $\partial\bar{\psi}/\partial\tilde{z}$, and we get $\partial\bar{\psi}/\partial\xi$ by a further change of coordinates to the elliptical ones linked with the advectee. Evaluating the resulting expression on the boundary of the advectee, $\bar{\Gamma}$, the resulting expression is easily integrated in (A1), and we obtain, after subtracting the part of $\dot{\phi}$ due to the advector alone [see Part I, Eq. (18)], the contribution to $\bar{\Omega}$ from an exterior ellipse:

$$\bar{\Omega} \leftarrow \omega'\epsilon'^2\lambda\cos 2(\phi-\phi')/(1-\lambda^2). \tag{A3}$$

For the external straining flow, the procedure is very similar. The external straining flow is prescribed by

$$\bar{\psi} = \tfrac{1}{4}(2\Omega zz^* - \gamma_s z^2 - \gamma_s^* z^{*2}), \tag{A4}$$

with $\gamma_s \equiv \gamma e^{-2i\phi_s}$, $\gamma(t)$ being the strain rate, $\phi_s(t)$ being the orientation of the strain axes, and $\Omega(t)$ being the background rotation. If we replace Ω by $\frac{1}{2}\omega'$ and γ_s by $\frac{1}{2}\omega'\epsilon'^2$ in (A4), the resulting equation becomes identical to (A2), the expression for the streamfunction inside an ellipse. Hence, it follows immediately that the straining flow contributes

$$\bar{\Omega} \leftarrow 2\gamma\lambda\cos 2(\phi-\phi_s)/(1-\lambda^2). \tag{A5}$$

When the advecting elliptical vortex (Z',λ',ϕ') is interior to the advected elliptical vortex (Z,λ,ϕ), the computations are significantly more demanding. Since the induced flow of the advector is irrotational, we may use to our advantage the complex extension of the streamfunction, namely,

$$\bar{\Psi}(w') = \kappa'(w' + \tfrac{1}{2}e^{-2w'}). \tag{A6}$$

The contribution to $\bar{\Omega}$ is then determined from a contour integral taken around the boundary of the advectee, $w = \bar{\Gamma} + i\eta$,

$$\Im\left[\frac{1}{2\pi}\int_{\bar{\Gamma}}^{\bar{\Gamma}+2i\pi}\frac{1}{\bar{h}^2}\frac{\partial\bar{\Psi}}{\partial w}dw\right] - \dot{\phi}. \tag{A7}$$

However, $\bar{\Psi}$ is a function of w', so we must change coordinates. A common point in the two coordinate systems is given by

$$Z' + c'e^{i\phi'}\cosh w' = Z + ce^{i\phi}\cosh w,$$

giving

$$\cosh w' = \Lambda\cosh w + (Z - Z')/2\nu', \tag{A8}$$

where

$$\nu \equiv \tfrac{1}{2}ce^{i\phi} \quad \text{and} \quad \lambda \equiv \nu/\nu'.$$

Hence, $dw'/dw = \Lambda\sinh w/\sinh w'$, and we can now calculate $\partial\bar{\Psi}/\partial w$ in (A7) by the chain rule. The result is

$$\frac{\partial\bar{\Psi}}{\partial w} = 2\kappa'\Lambda e^{-w'}\sinh w.$$

While w' still appears explicitly, the integration methods developed in Part I, Sec. V do not require any further substitutions. There is one last point that must be made before we can evaluate the integral in (A7). Note that $\partial\bar{\Psi}/\partial w$ evaluated along the boundary of the advectee will in general contain terms varying more rapidly than $\cos 2\eta$ and $\sin 2\eta$. In Part I, we neglected these higher-order terms in order to retain the part of the flow which would keep the advectee elliptical. Hence, in (A7), we are not justified in retaining terms in $\partial\bar{\Psi}/\partial w$ that vary more rapidly than $\cos 2\eta$ and $\sin 2\eta$. It follows that we can truncate the expansion of $\bar{h}^{-2}$ at the $\cos 2\eta$ term, i.e.,

$$\frac{1}{\bar{h}^2} \approx \frac{1}{R^2} + \frac{2}{R^2}\epsilon^2\cos 2\eta. \tag{A9}$$

Hence, we are left to calculate

$$\Re\left[\frac{\kappa' e^{i\phi'}}{2\pi\nu' R^2}\oint [1 + 2\epsilon^2\cosh 2(w-\bar{\Gamma})]e^{-w'}\,dz'\right] - \dot{\phi}. \tag{A10}$$

Now, since $2\cosh 2(w-\bar{\Gamma}) = \epsilon^2 e^{2w} + \epsilon^{-2}e^{-2w}$, the calculation reduces to finding the residues of $e^{-w'}$, $e^{-w'}e^{2w}$ and $e^{-w'}e^{-2w}$ (see Part I, Sec. V for general integration methods). The residue of $e^{-w'}$ is $\frac{1}{2}c'$, that of $e^{-w'}e^{2w}$ is $\frac{1}{2}c'[-2 + 1/\Lambda^2 + (Z-Z')^2/\nu^2]$, and that of $e^{-w'}e^{-2w}$ is 0. Combining these results and subtracting the part of $\dot{\phi}$ due to the advector alone [see Part I, Eq. (29)], we finally obtain

$$\overline{\Omega} \leftarrow \frac{\kappa'}{2R^2}\left\{2+(1+\epsilon^4)\Re\left[-2+\left(\frac{\nu'}{\nu}\right)^2+\left(\frac{Z-Z'}{\nu}\right)^2\right]\right\} \tag{A11}$$

as the contribution to $\overline{\Omega}$ from interior contours.

Finally, we turn to the contribution from separated ellipses. The procedure is quite similar to that just described for an interior ellipse. We can begin with Eq. (A10), with the understanding that the contour integration must be done differently (see Part I, Sec. VI). In fact, one cannot avoid the appearance of elliptic functions unless one approximates further. An accurate approximation is described in Part I, in which the advector is approximated by the effects of a finite set of point vortices lying along the line segment connecting the foci. Further details can be found in Part I, Sec. VI. In the following, it is sufficient to note that the strength of one of these approximating vortices will be denoted $\kappa_\odot$ and its position $z_\odot$.

The contour integral in question can be integrated exactly for each point vortex. The components of this integral have already turned up elsewhere [Sec. V, Eq. (22b)—J_0 and J_2 in particular], so it is easy to put these components together to obtain

$$\overline{\Omega} \leftarrow -(2\kappa_\odot/R^2)\epsilon^2 \sinh 2\overline{\Gamma}\,\Re(e^{-2\breve{w}_\odot}) - \dot{\phi},$$

[where $\cosh \breve{w}_\odot = (z_\odot - Z)/2\nu$]. Or, using the expression for $\dot{\phi}$ obtained in Part I, Eq. (39), we get

$$\overline{\Omega} \leftarrow -\frac{2\lambda}{1-\lambda^2}\frac{4\kappa_\odot}{c^2}\Re[e^{-2\breve{w}_\odot}] \tag{A12}$$

for the contribution from each point vortex within the advector. See Sec. VI for the complete expression for $\overline{\Omega}$.

APPENDIX B: GENERATION OF DISTURBANCES BY MISMATCHED FOCI

In this appendix, we present both an exact and an approximate calculation of the effects of mismatched foci. The exact calculation ultimately surrenders to a symbolic manipulation program, so a closed form expression for arbitrary m is not available. The approximate calculation is valid for all m, but it is then only approximate.

The task is to evaluate the integrals I_m and J_m defined by Eqs. (18) and (19). As shown in Part I, the problem reduces to finding the residue of a certain function, involving the product of $e^{-w'}$ and e^{mw} [see Part I, Sec. V, particularly Eq. (24) and the subsequent text]. Indeed, we have

$$J_m + iI_m = -\frac{\kappa'\epsilon^m}{\pi c}\oint e^{-w'(\tilde{z}')}e^{mw(\tilde{z}')}\,d\tilde{z}', \tag{B1}$$

using $\tilde{z}' \equiv (z - Z')e^{-i\phi'}$, i.e., the complex coordinate linked with the principal axes of the advector. Here $\tilde{z}'$ is related to w' through the relation $\tilde{z}' = c' \cosh w'$ (which may be regarded as a quadratic equation for $e^{-w'}$). Similarly, for the advectee, $\tilde{z} = c \cosh w$, so using the fact that z is the same point in both coordinate systems, we have $\tilde{z} = \tilde{z}'e^{i(\phi'-\phi)} + (Z' - Z)e^{-i\phi}$. We can therefore also express e^{mw} in terms of $\tilde{z}'$. The intermediate results are

$$e^{-w'} = \tilde{z}'/c' - \sqrt{(\tilde{z}'/c')^2 - 1}$$

and

$$e^{w} = \tilde{z}/c + \sqrt{(\tilde{z}/c)^2 - 1}.$$

The contour integral in (B1) can be taken around infinity, so we simply need to determine the coefficient of $1/\tilde{z}'$ in the expansion of $e^{-w'(\tilde{z}')}e^{mw(\tilde{z}')}$ for large $\tilde{z}'$. The value of the contour integral in (B1) is $2\pi i$ times this coefficient. If we introduce the notation $\varpi = c/\tilde{z}$ and $\varpi' = c'/\tilde{z}'$, then the problem is to determine the coefficient of ϖ' in the expansion of

$$F(\varpi') = 2\frac{1-\sqrt{1-\varpi'^2}}{\varpi'}\left(\frac{1+\sqrt{1-\varpi^2}}{\varpi}\right)^m \tag{B2}$$

for small ϖ', given

$$\frac{1}{\varpi} = \frac{P}{\varpi'} + \frac{Q}{2}, \tag{B3}$$

where $P \equiv 1/\Lambda = \nu'/\nu$ and $Q \equiv (Z' - Z)/\nu$. Denoting this coefficient by $G_m(P,Q)$, we have

$$J_m + iI_m = -i\kappa'\epsilon^m G_m(P,Q). \tag{B4}$$

Then, from (18), (19), and (B4), the contribution to $\dot{A}$ and $\dot{B}$ is

$$\dot{A} \leftarrow +\kappa'\epsilon^m \Im[G_m], \tag{B5a}$$

$$\dot{B} \leftarrow -\kappa'\epsilon^m \Re[G_m]. \tag{B5b}$$

We have not been able to find a closed form expression for $G_m(P,Q)$ for arbitrary m, so we have used a symbolic manipulation program (checked by hand up to $m = 4$) to calculate the first ten coefficients. These are

$$G_1 = Q,$$

$$G_2 = -2 + P^2 + Q^2,$$

$$G_3 = Q(-3 + 3P^2 + Q^2),$$

$$G_4 = 2 - 4P^2 + 2P^4 + Q^2(-4 + 6P^2 + Q^2),$$

$$G_5 = Q[5 - 15P^2 + 10P^4 + Q^2(-5 + 10P^2 + Q^2)],$$

$$G_6 = -2 + 9P^2 - 12P^4 + 5P^6 + Q^2(9 - 36P^2 + 30P^4) + Q^4(-6 + 15P^2 + Q^2),$$

$$G_7 = Q[-7 + 42P^2 - 70P^4 + 35P^6 + Q^2(14 - 70P^2 + 70P^4) + Q^4(-7 + 21P^2 + Q^2)],$$

$$G_8 = 2 - 16P^2 + 40P^4 - 40P^6 + 14P^8 + Q^2(-16 + 120P^2 - 240P^4 + 140P^6) + Q^4(20 - 120P^2 + 140P^4) + Q^6(-8 + 28P^2 + Q^2),$$

$$G_9 = Q[9 - 90P^2 + 270P^4 - 315P^6 + 126P^8 + Q^2(-30 + 270P^2 - 630P^4 + 420P^6) + Q^4(27 - 189P^2 + 252P^4) + Q^6(-9 + 36P^2 + Q^2)],$$

$$G_{10} = -2 + 25P^2 - 100P^4 + 175P^6 - 140P^8 + 42P^{10} + Q^2(25 - 300P^2 + 1050P^4 - 1400P^6 + 630P^8)$$
$$+ Q^4(-50 + 525P^2 - 1400P^4 + 1050P^6) + Q^6(35 - 280P^2 + 420P^4) + Q^8(-10 + 45P^2 + Q^2).$$

We can find a closed form expression if we introduce an approximation, namely to replace the advector by a finite string of point vortices distributed between the foci, just as we had done earlier in the separated ellipse calculations (see Part I, Sec. VI and Appendix A, and Sec. V in this paper). Denote the strength of one of these vortices by $\kappa_\odot$ and its position within the advector by $z_\odot$. Because each point vortex is contained within the advectee, the computation reduces to a contour integration taken around infinity. This computation, however, has already been done explicitly in Part I (Appendix B), it being a part of the computation required for the interaction of separated ellipses. The required integrals I_m and J_m can be taken over directly from Part I, Eq. (B1), restated here as

$$J_m + iI_m = -2i\kappa_\odot \epsilon^m \cosh m\breve{w}_\odot, \tag{B6}$$

with $\cosh \breve{w}_\odot = (z_\odot - Z)/2\nu$. Hence, the contribution to $\dot{A}$ and $\dot{B}$ from each point vortex is

$$\dot{A} \leftarrow J_m = +2\kappa_\odot \epsilon^m \Im[\cosh m\breve{w}_\odot], \tag{B7a}$$

$$\dot{B} \leftarrow I_m = -2\kappa_\odot \epsilon^m \Re[\cosh m\breve{w}_\odot]. \tag{B7b}$$

The seemingly close connection between (B7) and (B5) is bridged if we identify Q with $2\cosh \breve{w}_\odot$ and G_m with $2\cosh m\breve{w}_\odot$. With $G_0 = 2$ and $G_1 = Q$, the remaining G_m can be generated recursively by $G_{m+1} = QG_m - G_{m-1}$.

[1] B. Legras and D. G. Dritschel, Phys. Fluids A **3**, 845 (1991).
[2] H. H. Lamb, *Hydrodynamics* (Dover, New York, 1932).
[3] D. G. Dritschel, J. Fluid Mech. **210**, 223 (1990).
[4] S. Kida, J. Phys. Soc. Jpn. **50**, 3517 (1981).
[5] M. V. Melander, N. J. Zabusky, and A. S. Styczek, J. Fluid Mech. **167**, 95 (1986).
[6] M. V. Melander, J. C. McWilliams, and N. J. Zabusky, J. Fluid Mech. **178**, 137 (1987).
[7] B. Legras and D. G. Dritschel, submitted to J. Comput. Phys.
[8] D. W. Moore and P. G. Saffman, in *Aircraft Wake Turbulence and Its Detection*, edited by J. Olsen, A. Goldberg, and N. Rogers (Plenum, New York, 1971).
[9] D. G. Dritschel and B. Legras, submitted to J. Fluid Mech.
[10] P. G. Saffman and R. Szeto, Phys. Fluids **23**, 2339 (1980).
[11] D. G. Dritschel, J. Fluid Mech. **157**, 95 (1985).
[12] N. J. Zabusky, M. H. Hughes, and K. V. Roberts, J. Comput. Phys. **30**, 96 (1979).
[13] D. G. Dritschel, Comp. Phys. Rep. **10**, 77 (1989) and references therein.
[14] M. V. Melander, N. J. Zabusky, and J. C. McWilliams, J. Fluid Mech. **195**, 303 (1987).
[15] D. Waugh, Ph.D. thesis, University of Cambridge, England (in preparation).